

# UC Riverside

## UC Riverside Previously Published Works

### Title

Distinct Phenotypic Clusters of Glioblastoma Growth and Response Kinetics Predict Survival.

### Permalink

<https://escholarship.org/uc/item/5qv9357h>

### Authors

Rayfield, Corbin  
Grady, Fillan  
De Leon, Gustavo  
et al.

### Publication Date

2018-12-01

### DOI

10.1200/CCI.17.00080

Peer reviewed

# Distinct Phenotypic Clusters of Glioblastoma Growth and Response Kinetics Predict Survival

abstract

**Purpose** Despite the intra- and intertumoral heterogeneity seen in glioblastoma multiforme (GBM), there is little definitive data on the underlying cause of the differences in patient survivals. Serial imaging assessment of tumor growth allows quantification of tumor growth kinetics (TGK) measured in terms of changes in the velocity of radial expansion seen on imaging. Because a systematic study of this entire TGK phenotype—growth before treatment and during each treatment to recurrence—has never been coordinately studied in GBMs, we sought to identify whether patients cluster into discrete groups on the basis of their TGK.

**Patients and Methods** From our multi-institutional database, we identified 48 patients who underwent maximally safe resection followed by radiotherapy with imaging follow-up through the time of recurrence. The patients were then clustered into two groups through a *k*-means algorithm taking as input only the TGK before and during treatment.

**Results** There was a significant survival difference between the clusters ( $P = .003$ ). Paradoxically, patients among the long-lived cluster had significantly larger tumors at diagnosis ( $P = .027$ ) and faster growth before treatment ( $P = .003$ ) but demonstrated a better response to adjuvant chemotherapy ( $P = .048$ ). A predictive model was built to identify which cluster patients would likely fall into on the basis of information that would be available to clinicians immediately after radiotherapy (accuracy, 90.3%).

**Conclusion** Dichotomizing the heterogeneity of GBMs into two populations—one faster growing yet more responsive with increased survival and one slower growing yet less responsive with shorter survival—suggests that many patients who receive standard-of-care treatments may get better benefit from select alternative treatments.

Clin Cancer Inform. © 2018 by American Society of Clinical Oncology

## INTRODUCTION

Glioblastoma multiforme (GBM) is a highly aggressive and invasive primary brain tumor. With an annual incidence rate of 3.19/100,000, GBM remains the most common primary brain malignancy.<sup>1</sup> The current standard of care dictates that a patient with newly diagnosed GBM be treated with maximal safe resection, followed by a course of radiotherapy (RT) with concurrent and adjuvant temozolomide (TMZ).<sup>2</sup> After this standard first-line treatment, the progression of the disease is highly heterogeneous with a median survival of 14.6 months,<sup>3</sup> with 10% to 15% living to 3 years during the current standard-of-care era.<sup>4,5</sup>

Although there is a vast literature on intratumoral<sup>6</sup> and intertumoral heterogeneity<sup>7</sup> seen in GBM, there is little definitive data on the underlying

cause of the differences in survival in patients with GBM. Acknowledging that cancer is a complex evolving system of interacting populations of tumor cells and stroma, it is not surprising that molecular insights alone have failed to elucidate the full extent of the clinical heterogeneity we see across these patients. Recent studies have pointed to differences in tumor growth kinetics (TGK),<sup>8,9</sup> response to therapy,<sup>9-11</sup> genetic differences,<sup>12</sup> and tumor location,<sup>13</sup> along with the well-known predictors of age and Karnofsky performance status (KPS)<sup>14</sup> to explain some of the variance in outcomes. In addition, there have been some successes in connecting specific genotypic GBM variants and clinically relevant phenotypes. For example, patients with GBM who have a mutated isocitrate dehydrogenase 1 (IDH1) allele are typically younger and have improved survival outcomes.<sup>15</sup> One possible

Corbin A. Rayfield  
Fillan Grady  
Gustavo De Leon  
Russell Rockne  
Eduardo Carrasco  
Pamela Jackson  
Mayur Vora  
Sandra K. Johnston  
Andrea Hawkins-Daarud  
Kamala R. Clark-Swanson  
Scott Whitmire  
Mauricio E. Gamez  
Alyx Porter  
Leland Hu  
Luis Gonzalez-Cuyar  
Bernard Bendok  
Sujay Vora  
Kristin R. Swanson

Author affiliations and support information (if applicable) appear at the end of this article.

**Corresponding author:**  
Corbin A. Rayfield, MD,  
Mayo Clinic Arizona,  
5777 East Mayo Blvd,  
Support Services Building  
2-700, Phoenix, AZ  
85054; e-mail: rayfield.  
corbin@mayo.edu.

mechanism for this survival advantage may be related to a differing pattern of growth dominated by diffuse invasion of tumor cells with only modest proliferative capacity.<sup>16</sup> Another possible mechanism could be related to an increased radiosensitization<sup>17</sup> caused by increased sensitivity to oxidative damage.<sup>18</sup> Clinically, this has been shown to manifest itself through better RT response as determined by volumetric determinations of growth in IDH1 mutants.<sup>19</sup>

In this study, we hypothesized that the molecular diversity within and across tumors manifests as different tumor phenotypes that can be quantified as different TGK as seen on serial clinical magnetic resonance imaging (MRI) scans before and throughout therapy. Thus, we focus on elucidating the diversity in patient outcomes as it relates to this view of the dynamic imaging phenotype of each patient's tumor. Specifically, we sought to identify patterns of tumor growth and response kinetics that are consequential to clinical outcomes.

Performing clustering analysis of the TGK before and throughout treatment of this cohort of 48 similarly treated patients with GBM, we identified two discrete subgroups. We searched for underlying differences in the clinical presentation and response to early therapy that differentiates these subgroups and likely reflects an underlying biologic difference within the tumors. Finally, we attempted to use these baseline clinical differences to predict which subgroup a patient would fall into at the end of RT. To the best of our knowledge, this is the first time that TGK has been considered across the time course of patients from diagnosis through recurrence to detect clinically relevant phenotypic clusters that can explain a diversity of outcomes in GBM. In addition, this is the first study to attempt to connect the TGK across multiple domains, before treatment, and during therapy to the underlying mutational status of the patient.

## PATIENTS AND METHODS

### Patient Selection

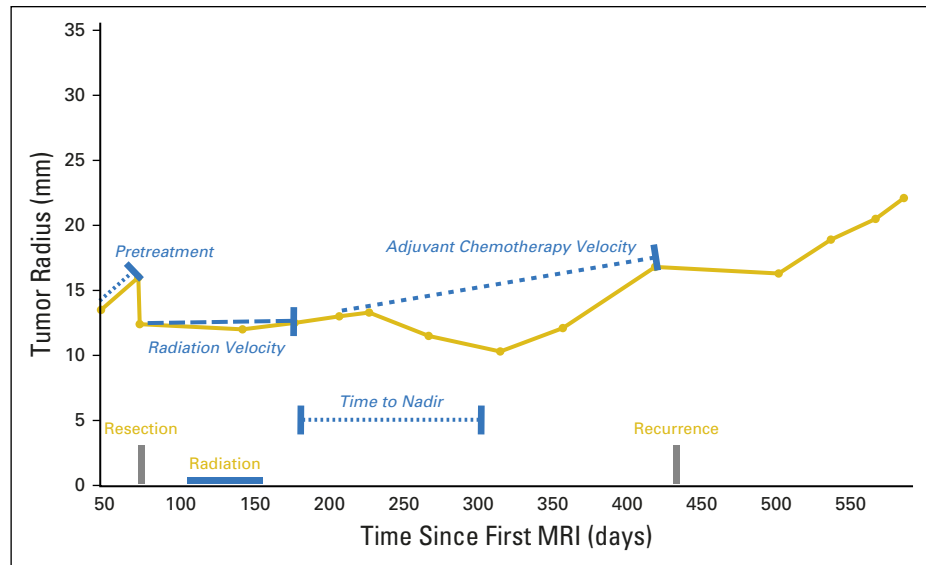
Forty-eight patients treated between 2002 and 2011 from our multi-institutional, prospective, institutional review board–approved database met the inclusion criteria of surgical intervention with histologic confirmation of newly diagnosed GBM and adjuvant RT to 60 Gy and observation

until radiographic progression such that all kinetic parameters could be calculated. This required that patients had at least two pretreatment MRI scans (separated by at least 4 days) and two MRI scans during adjuvant treatment before progression. Clustering analysis was performed on this group of 48 patients (referred to as the cluster cohort), and patients were then assigned to one of the two resultant clusters. To investigate phenotypic differences between cohorts, a smaller subcohort of 31 patients who received the current standard-of-care Stupp protocol (which includes maximal safe resection, RT concurrent with TMZ, and subsequent adjuvant TMZ) was also identified (standard Stupp cohort). The other 17 patients did not receive concurrent TMZ with RT but instead received TMZ as an adjuvant therapy after RT.

### Tumor Volume Delineation

Tumor volumes were measured on rate of longitudinal relaxation (T1)–weighted gadolinium-chelate–enhanced (T1Gd) and rate of transverse relaxation (T2) or fluid attenuation image recovery (FLAIR) MRI scans by using semiautomated threshold-based pixel intensity background subtraction software developed in MATLAB (Mathworks Software, Natick, MA). The range of acquisition parameters for the MRI scans are provided in the Appendix. The MRI tumor segmentations were performed by expert measurers trained in the technique. Quality of the segmentations was ensured by expert review by an additional reviewer. The accuracy and precision of this method has been shown to be comparable to or better than manual tumor delineation.<sup>20</sup> Specifically, the tumor volume  $V$  (cm<sup>3</sup>) was calculated by summing the volumes of the voxels marked as being tumor associated with each MRI scan. Each volume was then converted to a spherically equivalent radius which was then used to calculate the tumor kinetic parameters. Our focus on the use of spherically equivalent radius (extracted from the complex three-dimensional [3D] volume of the tumor) is a result of information from 20 years' worth of literature on the application of proliferation–invasion–based models for predicting glioma dynamics on clinical imaging.<sup>9-11,16,21-26</sup> These simple models incorporate a diffusion process for cellular migration and a logistic proliferative growth kinetic. Mathematically, this combination of diffusion and proliferation predicts, even within

**Fig 1.** Visual representation of the tumor growth kinetics calculated for each patient in the 48-patient cohort. Velocities were calculated according to a linear regression between two radii on rate of longitudinal relaxation-weighted gadolinium-chelate-enhanced and rate of transverse relaxation (or fluid attenuation image recovery) magnetic resonance imaging (MRI) scans. Time to nadir was calculated as the number of days between the end of radiation and the time at which the tumor radius was at its lowest point.



the context of the complex brain architecture, that the tumor radius visible on MRI scans evolves linearly in time. The same is not true of the volume; the volume would grow in a cubic fashion in this case. This constant velocity of linear radial expansion is termed a traveling wave, which means a wave that expands at a constant (traveling) rate. For this reason, several studies over the last 15 or more years have studied human gliomas with regard to their linear radial expansion.<sup>9-11,16,21-26</sup>

### Definition of Radial Velocities and Time to Nadir

For each patient, three possible TGK velocities were calculated: pretreatment, during RT, and during adjuvant chemotherapy (Fig 1). The tumor growth velocities were calculated by selecting two imaging events and performing linear regression according to:

$$Velocity = \frac{T1Gd_{radius2} - T1Gd_{radius1}}{t_2 - t_1}$$

Pretreatment velocities were calculated from T1Gd MRI scans that were at least 4 days apart before surgery or biopsy. RT velocities were calculated from T1Gd MRI scans taken before the start of RT (after surgery) and at 1 month after RT. Adjuvant chemotherapy velocity was calculated from the first T1Gd MRI scan before starting second-line therapy and the first image after RT at 1 month after treatment. Time to nadir was calculated by subtracting the date of the last RT treatment from the date of the smallest T1Gd tumor radius.

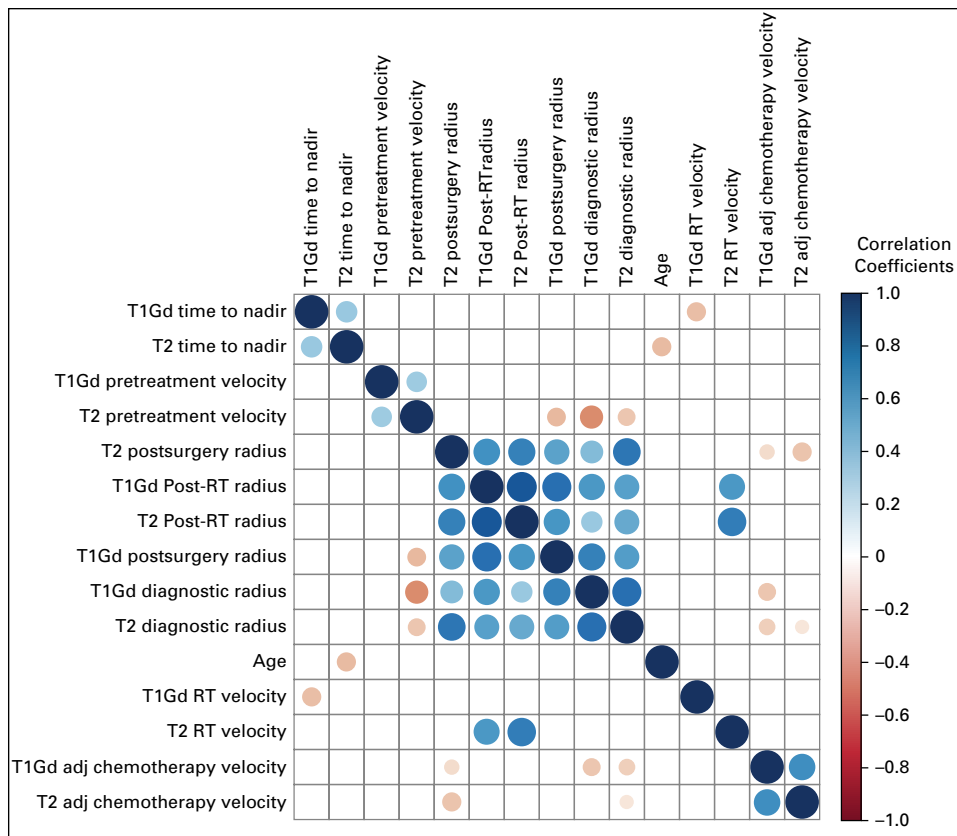
### Clustering Algorithm

The *k*-means algorithm was used to cluster patients according to inputs of T1Gd and T2 pretreatment growth velocity, T1Gd and T2 RT velocity, T1Gd and T2 adjuvant chemotherapy velocity, and T1Gd and T2 time to nadir. Time to nadir was the length of time that tumor growth was controlled on MRI scans. In short, the clustering algorithm finds patients with similar tumor kinetic parameters within this eight-dimensional space of the eight different measures of TGK considered as inputs.<sup>27</sup> That is to say, clusters are found that minimize the within-cluster variation as calculated by the Euclidean distance between individual tumor growth kinetic observations. In this case, patients were assigned a cluster so that the variation in growth kinetics within that cluster was minimized.

$$\min_{C_1, \dots, C_k} \left\{ \sum_{k=1}^K \frac{1}{|C_k|} \sum_{j=1}^p (x_{ij} - x_{i_j'})^2 \right\}$$

where  $C_k$  denotes the number of observations in the *k*th cluster, *K* indicates the number of clusters, and  $x_{ij} - x_{i_j'}$  is the Euclidean distance between parameter observations.<sup>28</sup> Before clustering, TGK metrics were scaled by dividing each value by the standard deviation of all observations so that parameters with large variability would not dominate the distance calculations. No other information about the patients except for the TGK measures was included at the time of clustering to prevent bias.

**Fig 2.** Correlations between tumor growth kinetics, size, and age for the full cohort. The color scale to the right indicates strength of correlation. All relationships indicated by a colored correlation are statistically significant ( $P < .05$ ). Tumor growth kinetics taken as markers of therapeutic response, such as time to nadir, adjuvant (adj) chemotherapy velocity, and radiotherapy (RT) velocity, show multiple significant correlations with tumor size and also with each other. For example, rate of longitudinal relaxation-weighted gadolinium-chelate-enhanced (T1Gd) time to nadir is negatively correlated with T1Gd RT velocity.



### Cluster Differences

Once clusters were defined, differences in clinical and imaging parameters between clusters among the whole cohort and the standard Stupp cohort were investigated by using  $t$  test and  $\chi^2$  tests performed in R (version 3.1.1). A full list of the clinical and imaging characteristics investigated is provided in Figure 2 for the clustering cohort. Survival differences between the clusters were investigated via a Cox proportional hazards model. Multivariable survival statistics included race, age, and KPS in addition to the variables being explored.  $P$  values less than .05 were considered to be significant, and because of the large number of comparisons investigated, all significant relationships were further tested with a Benjamini-Hochberg<sup>29</sup> procedure for multiple comparisons.

### Prediction Models

A flexible discriminate model was generated to predict which cluster prospective patients would likely fall into on the basis of information that would be available to the clinician immediately

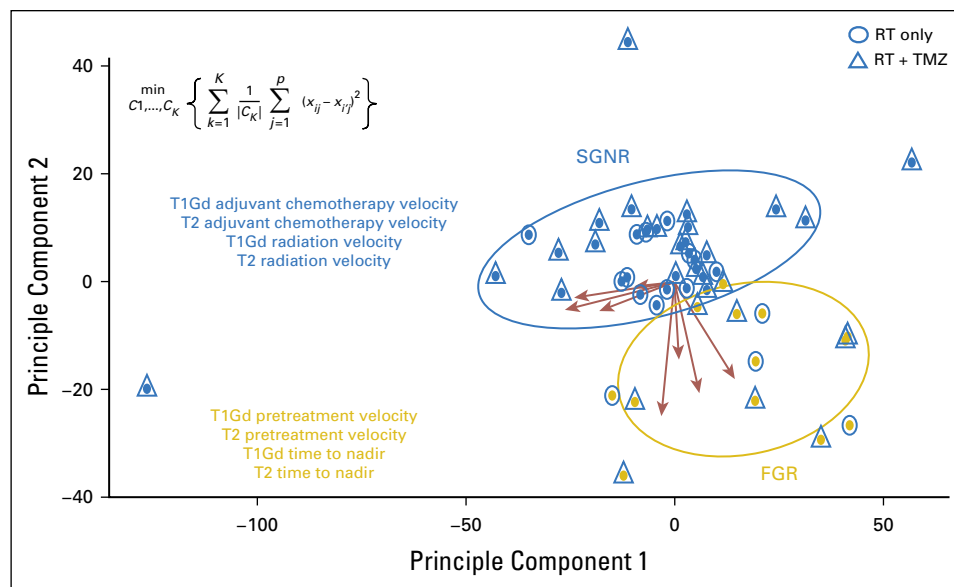
after RT: age, sex, KPS, hemisphere lateralization, T1Gd and T2 diagnostic radius, T1Gd and T2 postsurgical radius, the change in T1Gd and T2 radii from diagnosis to postsurgery, T1Gd and T2 post-RT radii, T1Gd and T2 pretreatment velocity, and T1Gd and T2 RT velocity. A flexible discriminate analysis model is a nonlinear classification model that, in this case, places new patients into the appropriate cluster on the basis of the probability of a patient with their given TGK being similar to the kinetic profile of the typical patient within that cluster.<sup>27</sup> This model was validated by using leave-one-out cross validation, and the accuracy, sensitivity, specificity, and  $P$  value comparing the model's prediction versus the no information rate (NIR) was reported. The NIR corresponded to the accuracy of prediction if all patients were assigned to the most prevalent cluster.

## RESULTS

### Cross Correlation of TGK Variables

First, correlations were sought that would indicate that the imaging and kinetic dynamics have

**Fig 3.** Patient clusters are shown within a two-dimensional space representative of the eight dimensions of different tumor growth kinetics parameters considered for the full cohort. Principle component analysis was used to extract information and represent the differences between patients in a two-dimensional plot. As the y-axis increases, rate of longitudinal relaxation-weighted gadolinium-chelate-enhanced (T1Gd)/rate of transverse relaxation (T2) pretreatment velocity and T1Gd/T2 time to nadir increase. Likewise, as the x-axis increases, the T1Gd/T2 adjuvant chemotherapy velocity and T1Gd/T2 radiotherapy (RT) velocity increase. Patients in this space seem closer than the actual distance function would calculate because the eight-dimensional space was shrunk to two dimensions for visual representation. Patients who received the Stupp protocol are represented by a triangle; patients who received RT alone are represented by a circle. The color of the patient dot indicates the clustering group. FGR, fast-growing responsive; SGNR, slow-growing nonresponsive; TMZ, temozolomide.



a significant relationship. As expected, tumor size on MRI scan (radius) at any time point was highly correlated with itself such that initial tumor size correlated with the size at recurrence. T2 pretreatment growth rate was inversely correlated with the initial tumor size at presentation on both T1Gd ( $R = -0.789$ ;  $P < .001$ ) and T2 ( $R = -0.577$ ;  $P = .001$ ; Fig 2). The velocity during radiation seen on T2 MRI, but not T1Gd, was correlated with the size of the lesion on both T1Gd ( $R = 0.596$ ;  $P = .008$ ) and T2 after RT ( $R = 0.637$ ;  $P = .004$ ). All significant correlations ( $P < .05$ ) between tumor characteristics are shown in Figure 2 for the cluster cohort and in Appendix Figure A1 for the standard Stupp cohort.

### k-Means Clustering Identifies Two Phenotypically Distinct Cohorts

k-means clustering was performed on the whole cohort and visualized by using principal component analysis (PCA; Fig 3). Two clusters were produced that had distinct TGK phenotypes visually separable according to the first two PCAs (Fig 3). The analogous PCA visualization for the standard Stupp subcohort (Appendix Figs A1 and A2) revealed a consistent association of the clusters to similar PCAs.

### Analysis of Clinical Parameters Between Clusters

Survival was significantly different between clusters for the Stupp patient cohort ( $P = .003$ ;

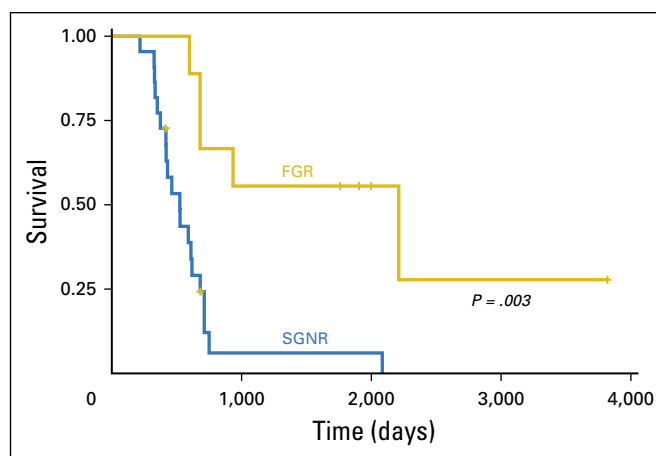
Fig 4). When considering the whole cohort, the significance of the survival difference was maintained ( $P < .001$ ; Appendix Fig A3). This significance between patients in the standard Stupp cohort increased on multivariable analysis with age, sex, and KPS (standard Stupp cohort  $P = .007$ ; whole cohort  $P < .001$ ). Cluster 1 had a median survival of 17.5 months, and cluster 2 had a median survival of 58.7 months for the standard Stupp cohort. Cluster 1 had 16 males and 6 females, and cluster 2 had 5 males and 4 females.

### Analysis of Imaging Characteristics Between Clusters

To investigate what made these patients in the standard Stupp clusters different, the patient's clinical and imaging characteristics were considered. Patients in cluster 1 compared with those in cluster 2 demonstrated significant differences in their tumors before therapeutic intervention (Table 1). Tumors from patients in cluster 1 were characterized as slow-growing nonresponsive (SGNR) therapeutically speaking, whereas tumors in patients in cluster 2 were fast growing responsive (FGR).

Specifically, tumors from patients in cluster 1 were marked by smaller tumor radii as measured on T1Gd and T2 MRI scans (13.68 v 18.50 mm;  $P = .031$  and 20.33 v 26.47 mm, respectively;  $P = .027$ ) and by slower growth before surgical resection (7.97 v 108.7 mm/year;

**Fig 4.** Kaplan-Meier curve showing the survival differences between clusters for the 31 patients in the standard Stupp cohort. Patients with tumors in the slow-growing nonresponsive (SGNR) cluster exhibited slower growth and minimal response to therapy whereas patients with tumors in the fast-growing responder (FGR) cluster demonstrated faster growth but a robust response to therapy. There was a significant difference in survival between the two clusters.



$P = .003$ ). In addition, cluster 1 patients had a lower response to chemotherapy as demonstrated in a larger adjuvant chemotherapy velocity on T1Gd MRI scans (22.00 v -13.94 mm/year;  $P = .048$ ), and cluster 1 time to nadir was shorter on both T1Gd and T2 MRI scans (122 v 588 days;  $P = .011$  and 73 v 248 days, respectively;  $P = .023$ ). Additional differences, none of which rose to the level of significance, are delineated in [Table 2](#).

#### Analysis of Pathologic Characteristics Between Clusters

Pathologic characteristics were compared to investigate the biologic basis that produced the apparent clustering phenotype on a limited cohort of patients with available tissue. None of the differences rose to the level of significance ([Table 2](#)). For the entire cohort, several trends toward significance were noted, specifically the vascular endothelial growth factor

(VEGF) staining extent and intensity ( $P = .15$ ) and the intensity of the hypoxia-inducible factor 1-alpha (HIF1 $\alpha$ ) staining ( $P = .12$ ; [Appendix Table A1](#)).

#### Building a Predictive Model for Clusters

A flexible discriminant analysis predictive model,<sup>27</sup> taking as inputs age, sex, KPS, hemisphere lateralization, T1Gd and T2 diagnostic radius, T1Gd and T2 postsurgical radius, the change in T1Gd and T2 radii from diagnosis to postsurgery, T1Gd and T2 post-RT radii, T1Gd and T2 pretreatment velocity, and T1Gd and T2 RT velocity was then generated on the standard Stupp cohort. The model, when tested for overfitting on a validation cohort produced via leave-one-out cross validation, demonstrated an accuracy of 90.3% in predicting whether a patient would fall into cluster 1 or 2. The sensitivity of this prediction was 90.9%, and the specificity was 88.9%. To test whether this prediction model was better than randomly guessing cluster group assignment, the accuracy was compared with the NIR (71.0%). The model was able to assign patients at a significantly better rate than the NIR ( $P = .010$ ).

To investigate what clinical parameters determined the predictive model clustering assignment, the relative variable importance was computed for each of the parameters within the model. The model was able to accurately differentiate patient clustering groups by using the pretreatment T1Gd velocity, T2 postsurgery radius, and the velocity during RT.

**Table 1.** Clinical Characteristics of Patients

Characteristic	No.	%
No. of patients	48	
Median age, years (range)	54 (20-76)	
Sex		
Male	29	60.4
Female	19	39.6
Median KPS at diagnosis (range)	90 (50-100)	
Resection treatment		
Gross total resection	25	52
Subtotal resection	14	29
Biopsy	9	19

Abbreviation: KPS, Karnofsky performance status.

**Table 2.** Differences Between Parameters for the 31 Patients in the SGNR and FGR Clusters for the Standard Care Stupp Cohort

Parameter	Median SGNR	Median FGR			P
		mm/Year	mm	Days	
T1Gd pretreatment velocity	7.97	108.70			.00
T1Gd time to nadir	122			588	.01
T2 time to nadir	73			248	.02
T2 diagnostic radius	20.33		26.47		.03
T1Gd diagnostic radius	13.68		18.50		.03
T1Gd adjuvant chemotherapy velocity	22.00	-13.94			.05
T1Gd postsurgical radius	12.34		15.38		.14
T2 postsurgical radius	20.28		22.24		.33
T1Gd radial change postsurgery	1.33		3.11		.35
T2 radial change postsurgery	1.96		3.51		.36
T1Gd postradiation radius	12.10		14.11		.37
T2 RT velocity	-0.143	-8.14			.46
T2 post-RT radius	17.54		19.75		.54
Extent of surgery	NA	NA	NA		.78
T2 pretreatment velocity	-36.06	-17.27			.80
Hemisphere lateralization	NA	NA	NA		.80
T2 adjuvant chemotherapy velocity	25.23	21.35			.88
T1Gd RT velocity	-10.97	-10.87			.99

NOTE. Patients with FGR tumors with significantly longer survival had significant differences among rate of longitudinal relaxation-weighted gadolinium-chelate-enhanced (T1Gd) pretreatment velocity ( $P = .00$ ), T1Gd time to nadir ( $P = .01$ ), rate of transverse relaxation (T2) time to nadir ( $P = .02$ ), T2 diagnostic radius ( $P = .03$ ), and T1Gd adjuvant chemotherapy velocity ( $P = .05$ ). These significant differences were those that remained on correction for multiple comparisons.

Abbreviations: FGR, fast-growing responsive; NA, not applicable; RT, radiotherapy; SGNR, slow-growing nonresponsive.

## DISCUSSION

To the best of our knowledge, this research represents the first time that the dynamics of TGK have been considered from diagnosis through recurrence in GBM. In this study, we have shown that patients can be clustered into two distinct clinical phenotypes. These two clusters of patients have a different outcome profile and differ in their tumor size and TGK. Specifically, those patients (SGNR cluster 1) who have a lower median survival demonstrate smaller tumors with less aggressive growth kinetics, but they show a very poor response to therapy. Patients in the other cluster (FGR cluster 2) showed opposite characteristics. These patients had faster growing tumors and had a larger edematous lesion on diagnosis but had an excellent response to therapy as demonstrated

by their negative T1Gd adjuvant chemotherapy velocity and longer T1Gd and T2 time to nadir.

Our results indicate that patients with tumors that exhibit brisk growth before intervention are the same patients that demonstrate a significant response to adjuvant chemotherapy. Interestingly, the more aggressive yet more responsive FGR cluster portended for better survival than the intrinsically less aggressive but unresponsive SGNR cluster. This suggests that the long tail apparent on the survival curves in the Stupp era<sup>3</sup> may be dominated by patients with aggressive tumors before treatment with unusually significant response kinetics to TMZ (FGR group). Although O(6)-methylguanine-DNA methyltransferase (MGMT) methylation status was not available for all the patients in our cohort, it is notable that MGMT methylation status did not seem to differentiate these clusters, which suggests that alternative biologic mechanisms may be at play. Thus, these results further suggest that TGK may serve as an important tool for discovery of previously unknown biologic, cellular, and molecular drivers of this enhanced response among patients that fit the FGR phenotype.

Our results further reiterate the need for strong response metrics that can identify effective treatment response early in treatment. Other recent research has shown the importance of considering TGK in the evaluation of treatment response.<sup>10,11</sup> Data from phase I clinical trials have shown that the TGK can be an early prognostic indicator of chemotherapy effectiveness and that the comparison of pretreatment to therapeutic growth kinetics is a more sensitive indicator of efficacy than the standard Response Assessment in Neuro-Oncology Criteria.<sup>30-32</sup> Similarly, data from patients treated with epidermal growth factor receptor (EGFR) tyrosine kinase inhibitors demonstrated that the TGK during the treatment period were highly correlated with both overall survival and time to progression.<sup>33</sup> In renal cell carcinomas, the rate of tumor growth has been used to successfully determine candidates for salvage therapy versus active surveillance after percutaneous thermal ablation.<sup>34</sup> All of these studies underscore the need for more dynamic insight into treatment response that incorporates knowledge of the underlying untreated/pretreatment tumor behavior.

Significant progress has been made to delineate the genetic heterogeneity that GBM tumors

exhibit. Genome-wide methylation profiling has shown that within IDH-mutant GBM tumors, different subtypes exist and that the clinical outcome among subtypes is also significantly different.<sup>35</sup> In addition, large-scale genomic characterization of data from The Cancer Genome Atlas has shown that at least four subtypes of GBM tumors exist: proneural, neural, classic, and mesenchymal.<sup>36</sup> Only one of these subtypes (proneural) distinguishes itself as having a different median survival.<sup>7</sup> These studies have greatly advanced our understanding of the mutations that drive GBM tumor growth, but the connection of these mutations to TGK and particularly to individualized treatment response is still missing.

Although every effort has been made to ensure accurate data collection and analysis, there are several potential limitations in this study. Velocity measurements are subject to small but measurable interobserver variability that could affect the classification of TGK. In addition, pseudoprogression was controlled for within the postadjuvant chemotherapy velocity by selecting the last MRI before a change in systemic therapy to a second-line agent, re-irradiation, or resection. There are also concerns about whether the T2/FLAIR sequence correlates with tumor activity after chemoradiation because of the inflammatory response these treatments induce. We have studied the variability among measurements for our group, and we find that the average variation is within 0.3 mm. The greatest degree of uncertainty comes from the pretreatment velocity measurements because of the minimal separation between imaging events. To reduce the error as much as possible, we limit inclusion to only those that are separated by 4 or more days. In addition, comparisons of pathologic characteristics were limited by the number of patients who

had available tissue. Ideally, MGMT status would be known for a larger proportion of the patients, but because of the time at which these patients were treated, this was not a standard investigation. Although this study moves our understanding of TGK in GBM forward, there is still much work to be done. Likely because of the limited availability of patient tissue, we were unable to find differences in the staining for common genetic variants between the clusters. It will be necessary to correlate these TGK phenotypes with further molecular and histologic characterization.

To the best of our knowledge, the systemic study of the entire TGK phenotype—growth before treatment and during each treatment to recurrence—has never been studied in a coordinated way in GBM. In this study, we revealed two important TGK phenotypes, one more aggressive but benefiting strongly from treatment and another that has a more benign natural history with minimal treatment response. This provides insight into the interpatient heterogeneity we see in patient outcomes. Furthermore, the proposed preliminary predictive models support the possibility of identifying, before or early in treatment, the patients who are likely to receive durable response and thus improved survival. These results strongly support the value of insightful response metrics that meaningfully connect early measures of degree of response with those patient-specific outcomes. We conclude that a dynamic view of GBM growth and response kinetics is essential to progress in delivering successful patient-individualized precision medicine strategies.

DOI: <https://doi.org/10.1200/CCI.17.00080>

Published online on [ascopubs.org/journal/cci](https://ascopubs.org/journal/cci) on March 1, 2018.

#### CONTRIBUTIONS

**Conception and design:** Corbin A. Rayfield, Fillan Grady, Gustavo De Leon, Russell Rockne, Pamela Jackson, Leland Hu, Bernard Bendok, Kristin R. Swanson

**Financial support:** Corbin A. Rayfield, Kristin R. Swanson

**Administrative support:** Corbin A. Rayfield, Gustavo De Leon

**Provision of study materials or patients:** Corbin A. Rayfield, Scott Whitmire

**Collection and assembly of data:** Corbin A. Rayfield, Fillan Grady, Eduardo Carrasco, Pamela Jackson, Mayur Vora, Sandra K. Johnston, Kamala R. Clark-Swanson, Scott Whitmire, Luis Gonzalez-Cuyar, Bernard Bendok, Kristin R. Swanson

**Data analysis and interpretation:** Corbin A. Rayfield, Fillan Grady, Eduardo Carrasco, Pamela Jackson, Sandra K. Johnston, Andrea Hawkins-Daarud, Scott Whitmire, Mauricio E. Gamez, Alyx Porter, Leland Hu, Bernard Bendok, Sujay Vora, Kristin R. Swanson

**Manuscript writing:** All authors

**Final approval of manuscript:** All authors

**Accountable for all aspects of the work:** All authors

#### AUTHORS' DISCLOSURES OF POTENTIAL CONFLICTS OF INTEREST

The following represents disclosure information provided by authors of this manuscript. All relationships are considered compensated. Relationships are self-held

unless noted. I = Immediate Family Member, Inst = My Institution. Relationships may not relate to the subject matter of this manuscript. For more information about ASCO's conflict of interest policy, please refer to [www.asco.org/rwc](http://www.asco.org/rwc) or [ascopubs.org/jco/site/ifc](http://ascopubs.org/jco/site/ifc).

**Corbin A. Rayfield**  
No relationship to disclose

**Fillan Grady**  
No relationship to disclose

**Gustavo De Leon**  
No relationship to disclose

**Russell Rockne**  
No relationship to disclose

**Eduardo Carrasco**  
No relationship to disclose

**Pamela Jackson**  
No relationship to disclose

**Mayur Vora**  
No relationship to disclose

**Sandra K. Johnston**  
No relationship to disclose

**Andrea Hawkins-Daarud**  
No relationship to disclose

**Kamala R. Clark-Swanson**  
**Employment:** Mayo Clinic  
**Patents, Royalties, Other Intellectual Property:** Method and system for determining the spatial extent, aggressiveness, and other characteristics of various types of tumors, using parameterized computational models and medical imaging technology, US 8571844B2 (I)

**Scott Whitmire**  
**Stock and Other Ownership Interests:** IBM, GE Healthcare

**Mauricio E. Gamez**  
No relationship to disclose

**Alyx Porter**  
No relationship to disclose

**Leland Hu**  
No relationship to disclose

**Luis Gonzalez-Cuyar**  
No relationship to disclose

**Bernard Bendock**  
No relationship to disclose

**Sujay Vora**  
No relationship to disclose

**Kristin R. Swanson**  
No relationship to disclose

#### ACKNOWLEDGMENTS

We thank Alex Kim, April Baldock, Christine Scullywest, Chunyan Zhou, Danielle Peacock, Jacob Gile, Jon Hagg, Julia Hamilton, Sam Sussman, Shokouh Pardakhtim, Tyler Cloke, Tyler Rockhill, and Josh Jacobs for their help with tumor delineation and measurement and for technical assistance. We especially recognize the lasting impact that Anne Baldock (1991-2015) made on this project, in our lives, in the lives of the patients that she impacted, and those she never had a chance to help. We gratefully acknowledge the generous and unwavering support of Ellsworth (Buster) C. Alvord Jr (1923-2010) who is gravely missed. May his scientific legacy live on through work like that reported here.

#### Affiliations

**Corbin A. Rayfield, Fillan Grady, Gustavo De Leon, Eduardo Carrasco, Pamela Jackson, Mayur Vora, Sandra K. Johnston, Andrea Hawkins-Daarud, Kamala R. Clark-Swanson, Scott Whitmire, Mauricio E. Gamez, Alyx Porter, Leland Hu, Bernard Bendok, Sujay Vora, and Kristin R. Swanson,** Mayo Clinic, Phoenix, AZ; **Russell Rockne,** Beckman Research Institute, City of Hope, Duarte, CA; and **Sandra K. Johnston and Luis Gonzalez-Cuyar,** University of Washington, Seattle, WA

#### Support

Supported by the James S. McDonnell Foundation, the Ivy Foundation, Mayo Clinic, the James D. Murray Endowed Chair, and National Institutes of Health Grants No. R01NS060752, R01CA164371, U54CA210180, U54CA143970, U54CA193489, and U01CA220378.

#### REFERENCES

1. Ostrom QT, Gittleman H, Liao P, et al: CBTRUS statistical report: Primary brain and central nervous system tumors diagnosed in the United States in 2007-2011. *Neuro Oncol* 16:iv1-iv63, 2014
2. Stupp R, Mason WP, van den Bent MJ, et al: Radiotherapy plus concomitant and adjuvant temozolomide for glioblastoma. *N Engl J Med* 352:987-996, 2005
3. Stupp R, Hegi ME, Mason WP, et al: Effects of radiotherapy with concomitant and adjuvant temozolomide versus radiotherapy alone on survival in glioblastoma in a randomised phase III study: 5-year analysis of the EORTC-NCIC trial. *Lancet Oncol* 10:459-466, 2009

4. McNamara MG, Lwin Z, Jiang H, et al: Conditional probability of survival and post-progression survival in patients with glioblastoma in the temozolomide treatment era. *J Neurooncol* 117:153-160, 2014
5. Smoll NR, Schaller K, Gautschi OP: Long-term survival of patients with glioblastoma multiforme (GBM). *J Clin Neurosci* 20:670-675, 2013
6. Kumar A, Boyle EA, Tokita M, et al: Deep sequencing of multiple regions of glial tumors reveals spatial heterogeneity for mutations in clinically relevant genes. *Genome Biol* 15:530, 2014
7. Verhaak RG, Hoadley KA, Purdom E, et al: Integrated genomic analysis identifies clinically relevant subtypes of glioblastoma characterized by abnormalities in PDGFRA, IDH1, EGFR, and NF1. *Cancer Cell* 17:98-110, 2010
8. Wang CH, Rockhill JK, Mrugala M, et al: Prognostic significance of growth kinetics in newly diagnosed glioblastomas revealed by combining serial imaging with a novel biomathematical model. *Cancer Res* 69:9133-9140, 2009
9. Rockne R, Rockhill JK, Mrugala M, et al: Predicting the efficacy of radiotherapy in individual glioblastoma patients in vivo: A mathematical modeling approach. *Phys Med Biol* 55:3271-3285, 2010
10. Neal ML, Trister AD, Ahn S, et al: Response classification based on a minimal model of glioblastoma growth is prognostic for clinical outcomes and distinguishes progression from pseudoprogression. *Cancer Res* 73:2976-2986, 2013
11. Neal ML, Trister AD, Cloke T, et al: Discriminating survival outcomes in patients with glioblastoma using a simulation-based, patient-specific response metric. *PLoS One* 8:e51951, 2013
12. Mazaris P, Hong X, Altshuler D, et al: Key determinants of short-term and long-term glioblastoma survival: A 14-year retrospective study of patients from the Hermelin Brain Tumor Center at Henry Ford Hospital. *Clin Neurol Neurosurg* 120:103-112, 2014
13. Adeberg S, Bostel T, König L, et al: A comparison of long-term survivors and short-term survivors with glioblastoma, subventricular zone involvement: A predictive factor for survival? *Radiat Oncol* 9:95, 2014
14. Li J, Wang M, Won M, et al: Validation and simplification of the Radiation Therapy Oncology Group recursive partitioning analysis classification for glioblastoma. *Int J Radiat Oncol Biol Phys* 81:623-630, 2011
15. Parsons DW, Jones S, Zhang X, et al: An integrated genomic analysis of human glioblastoma multiforme. *Science* 321:1807-1812, 2008
16. Baldock AL, Ahn S, Rockne R, et al: Patient-specific metrics of invasiveness reveal significant prognostic benefit of resection in a predictable subset of gliomas. *PLoS One* 9:e99057, 2014
17. Li S, Chou AP, Chen W, et al: Overexpression of isocitrate dehydrogenase mutant proteins renders glioma cells more sensitive to radiation. *Neuro Oncol* 15:57-68, 2013
18. Zhao S, Lin Y, Xu W, et al: Glioma-derived mutations in IDH1 dominantly inhibit IDH1 catalytic activity and induce HIF-1 $\alpha$ . *Science* 324:261-265, 2009
19. Tran AN, Lai A, Li S, et al: Increased sensitivity to radiochemotherapy in IDH1 mutant glioblastoma as demonstrated by serial quantitative MR volumetry. *Neuro Oncol* 16:414-420, 2014
20. Joe BN, Fukui MB, Meltzer CC, et al: Brain tumor volume measurement: Comparison of manual and semiautomated methods. *Radiology* 212:811-816, 1999
21. Swanson K: Mathematical modeling of the growth and control of tumors [doctoral thesis]. University of Washington, Seattle, WA, 1999
22. Jackson PR, Juliano J, Hawkins-Daarud A, et al: Patient-specific mathematical neuro-oncology: Using a simple proliferation and invasion tumor model to inform clinical practice. *Bull Math Biol* 77:846-856, 2015
23. Baldock AL, Rockne RC, Boone AD, et al: From patient-specific mathematical neuro-oncology to precision medicine. *Front Oncol* 3:62, 2013

24. Swanson KR, Harpold HL, Peacock DL, et al: Velocity of radial expansion of contrast-enhancing gliomas and the effectiveness of radiotherapy in individual patients: A proof of principle. *Clin Oncol* 20:301-308, 2008
25. Corwin D, Holdsworth C, Rockne RC, et al: Toward patient-specific, biologically optimized radiation therapy plans for the treatment of glioblastoma. *PLoS One* 8:e79115, 2013
26. Swanson KR, Rostomily RC, Alvord EC Jr: A mathematical modelling tool for predicting survival of individual patients following resection of glioblastoma: A proof of principle. *Br J Cancer* 98:113-119, 2008
27. Hastie T, Tibshirani R, Friedman J: *The Elements of Statistical Learning: Data Mining, Inference, and Prediction* (ed 2). New York, NY, Springer Science+Business Media, 2009
28. James G, Witten D, Hastie T, et al: *An Introduction to Statistical Learning: With Applications in R*. New York, NY, Springer, 2013
29. Benjamini Y, Hochberg Y: Controlling the false discovery rate: A practical and powerful approach to multiple testing. *J R Stat Soc B* 57:289-300, 1995
30. Adair JE, Johnston SK, Mrugala MM, et al: Gene therapy enhances chemotherapy tolerance and efficacy in glioblastoma patients. *J Clin Invest* 124:4082-4092, 2014
31. Ferte C, Fernandez M, Hollebecque A, et al: Tumor growth rate is an early indicator of antitumor drug activity in phase I clinical trials. *Clin Cancer Res* 20:246-252, 2014
32. Wen PY, Macdonald DR, Reardon DA, et al: Updated response assessment criteria for high-grade gliomas: Response assessment in neuro-oncology working group. *J Clin Oncol* 28:1963-1972, 2010
33. Lee JH, Lee HY, Ahn MJ, et al: Volume-based growth tumor kinetics as a prognostic biomarker for patients with EGFR mutant lung adenocarcinoma undergoing EGFR tyrosine kinase inhibitor therapy: A case control study. *Cancer Imaging* 16:5, 2016
34. Chen JX, Maass D, Guzzo TJ, et al: Tumor Growth Kinetics and Oncologic Outcomes of Patients Undergoing Active Surveillance for Residual Renal Tumor following Percutaneous Thermal Ablation. *J Vasc Interv Radiol* 27:1397-1406, 2016
35. Ceccarelli M, Barthel FP, Malta TM, et al: Molecular profiling reveals biologically discrete subsets and pathways of progression in diffuse glioma. *Cell* 164:550-563, 2016
36. Brennan CW, Verhaak RG, McKenna A, et al: The somatic genomic landscape of glioblastoma. *Cell* 155:462-477, 2013

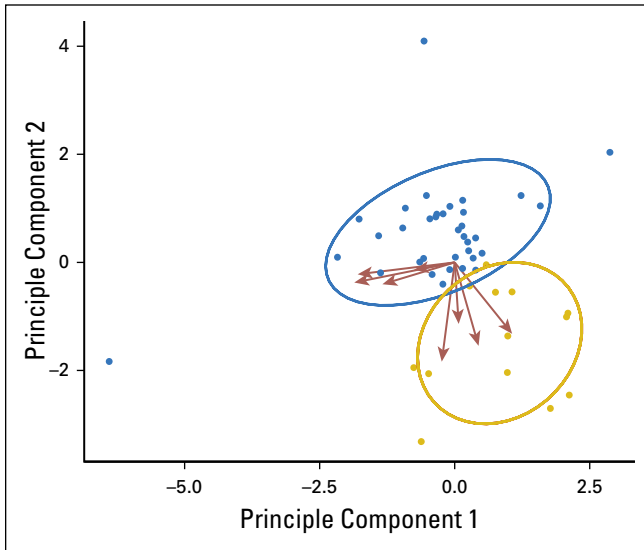


**Fig A1.** Patient clusters are shown within a two-dimensional space representative of the eight dimensions of different tumor growth kinetics parameters considered for the Stupp cohort.

**Work Flow**

Patients were selected from a retrospective database if they met the following criteria: pathologic diagnosis of glioblastoma; received surgical intervention, radiotherapy (RT), and adjuvant chemotherapy; and had enough imaging time points that all eight tumor growth kinetics could be calculated. The tumor growth kinetics were calculated by taking the slope of the line connecting the imaging points which corresponded to pretreatment, during RT, or during adjuvant chemotherapy.

Patients were clustered according to their tumor growth kinetics. The specific clustering algorithm used was a *k*-means algorithm implemented in the R statistical programming language (Package stats version 3.4.0; R version 3.4.1). Clustering was performed only on the following eight variables: among rate of longitudinal relaxation-weighted gadolinium-chelate-enhanced (T1Gd) and rate of transverse relaxation (T2) pretreatment growth velocity, T1Gd and T2 RT velocity, T1Gd and T2 adjuvant chemotherapy velocity, and T1Gd and T2 time to nadir.

Once clustered, any significant differences between the clusters were investigated for all available clinical and imaging parameters (see [Table 1](#) for a complete list) among the whole cohort. This analysis was again performed for only those patients who received concurrent temozolomide along with RT.

A prediction model was generated by using a flexible discriminant analysis implemented in the R statistical programming language (Package caret version 6.0-77, R version 3.4.1) to test whether a prospective patients cluster could be predicted on the basis of information available immediately after the conclusion of RT.

**Fig A2.** Correlations between tumor growth kinetics, size, and age for patients in the standard Stupp cohort. The color scale to the right indicates strength of correlation. All relationships indicated by a colored correlation are statistically significant ( $P < .05$ ). RT, radiotherapy.

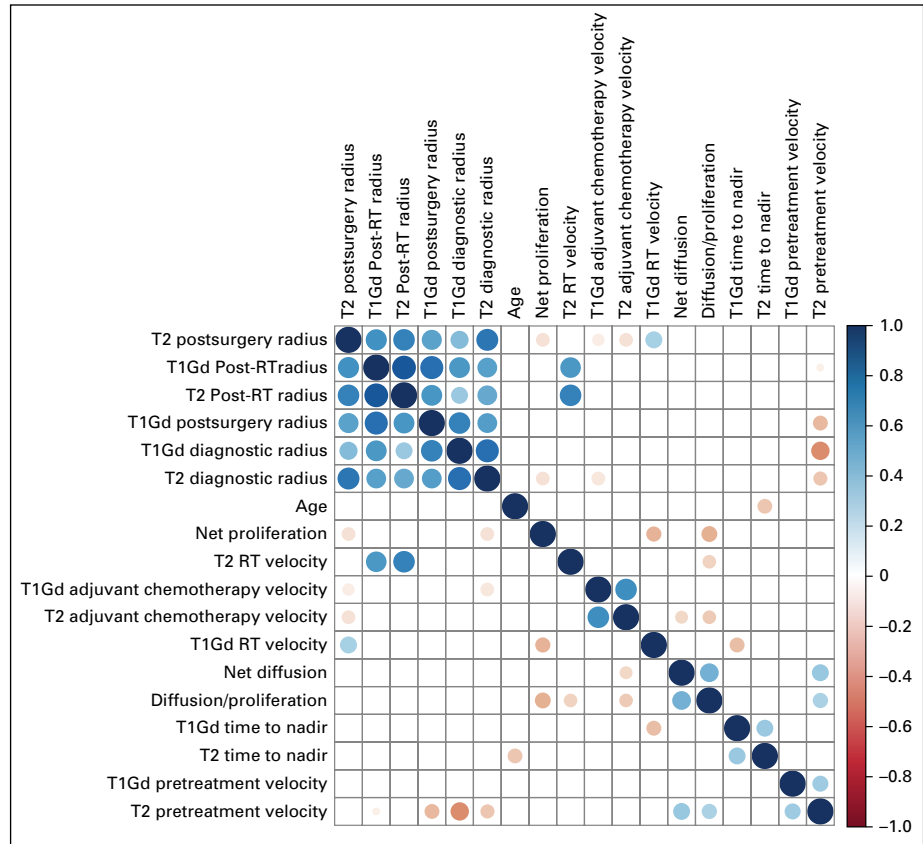


**Fig A3.** Kaplan-Meier survival curve for the whole 48-patient cohort. Patients with fast-growing responsive (FGR) tumors had significantly longer survival than patients with slow-growing nonresponsive (SGNR) tumors.

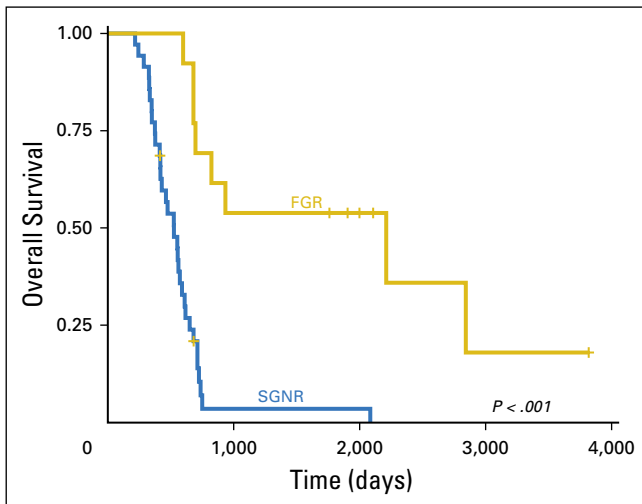


**Table A1.** Differences in Immunohistochemistry Staining for SGNR Versus FGR Patients in the Standard Care Stupp Cohort

<b>Pathology Parameter</b>	<b>No. of Patients</b>	<b>P</b>
Staining extent		
PDGFRa	11	.49
VEGF	11	.59
HIF1a	11	.59
Staining intensity		
VEGF	11	.50
HIF1a	11	.50
PDGFRa	11	.66
MGMT	5	.82

NOTE. No parameters examined exhibited statistically significant differences.

Abbreviations: FGR, fast-growing responsive; HIF1 $\alpha$ , hypoxia-inducible factor 1-alpha; MGMT, O(6)-methylguanine-DNA methyltransferase; PDGFRa, platelet-derived growth factor receptor a; SGNR, slow-growing nonresponsive; VEGF, vascular endothelial growth factor.